

Recombination dynamics of excitons bound to nitrogen isoelectronic centers in δ -doped GaPP. St-Jean,^{1,*} G. Éthier-Majcher,¹ Y. Sakuma,² and S. Francoeur¹¹*Polytechnique Montréal, Montréal, Québec H3C 3A7, Canada*²*National Institute for Materials Science, 1-1 Namiki, Tsukuba 305-0044, Japan*

(Received 3 July 2013; revised manuscript received 20 December 2013; published 19 February 2014)

Using time-resolved luminescence, we report on the recombination lifetime of excitons bound to nitrogen isoelectronic centers (ICs) in δ -doped GaP. For all ICs considered (A line and NN_i , with $i = 1, 3, 4, 6$), the recombination lifetime is identical for all transitions composing the fine structure, indicating a fast transfer between all eight excitonic states. From 5 to 60 K, the lifetime decreases by three orders of magnitude and is characterized by three distinct regimes successively dominated by (1) transfers between thermally mixed bright and dark states, (2) hole escape for $i \leq 4$ or exciton escape for $i \geq 6$ and the A line, and (3) exciton capture through hopping from single nitrogen centers to nitrogen dyads. Improving on previous population balance models to include both light- and heavy-hole states, we accurately reproduce this temperature evolution of the lifetime and quantify the radiative lifetime of all transitions, the energy position of dark states, and the exciton capture time.

DOI: [10.1103/PhysRevB.89.075308](https://doi.org/10.1103/PhysRevB.89.075308)

PACS number(s): 78.47.jd, 78.67.-n, 71.35.-y, 71.55.-i

I. INTRODUCTION

Over the last decade, considerable interest has been devoted to the implementation of single-electron and single-exciton storing devices for classical and quantum information processing. Storage has been achieved in various systems such as epitaxial quantum dots [1,2], nitrogen-vacancy centers in diamond [3,4], and phosphorous donors in silicon [5,6], leading to impressive realizations such as atomic-size memories and single-qubit initialization and manipulation. Further developing these systems beyond these first demonstrations remains however a challenging task: electrostatically defined quantum dots only operate at extremely low temperatures, phosphorous donors in silicon cannot be addressed optically, self-assembled quantum dots suffer from large inhomogeneous broadening, and NV centers in diamond are difficult to integrate in semiconductor devices.

Interestingly, the number of atomic impurities, such as dopants and color centers, is truly impressive and a number of them could be equally suitable or more advantageous than those already actively investigated. If many impurity-host systems have already been extensively studied, it was most often in a different context and with different objectives. It may therefore prove advantageous to revisit some of them, determine whether they can be addressed and probed individually, and explore their respective advantages for their use as building blocks for the implementation of quantum functionalities. Isoelectronic impurities in semiconductors are interesting candidates as they may provide some of the required characteristics.

Isoelectronic centers (ICs) are isovalent impurities that can trap, through a disruption in electronic charge density of the host semiconductor crystal, either an electron or hole depending on the electronegativity of the impurity. Then, this primary charge can trap an itinerant charge of the opposite sign to form a bound exciton. The ability to optically resolve a single IC has been demonstrated for nitrogen dyads in GaAs [7], AlAs [8], and GaP [9] and for tellurium dyads

in ZnSe [10,11]. Many of their characteristics are reminiscent of quantum dots, since they can bind excitons, biexcitons, and charged excitons [12], they can be addressed both optically and electrically, and their properties can be tuned by varying the number of atoms composing the IC. However, in contrast to quantum dots, their atomic dimension provides atomically sharp emission lines free of inhomogeneous broadening and well-defined symmetries, both of which are highly desirable for most applications.

Extensively studied several decades ago for applications as light-emitting diodes, N isoelectronic centers in GaP are probably the most well understood isoelectronic impurities in III-V semiconductors. They are also one of the most interesting impurity-host systems, since a large variety of IC configurations can be directly observed: the single-nitrogen IC, several dyads with various interatomic separations [13], and other configurations involving three or more isoelectronic impurities [14] all emit within the forbidden gap. However, a critical aspect for the realization of single-charge storage and its exploitation for computation schemes is a complete understanding of the exciton dynamics, which we address in this work.

We report a detailed study of the recombination dynamics of excitons bound to various nitrogen isoelectronic centers (ICs) in gallium phosphide. Using samples with very low nitrogen concentrations, we measured the time dependence of the photoluminescence intensity of several configurations (single-atom configuration and dyads with various interatomic distances) as a function of temperature. By modeling our data with a numerical simulation of the excitonic populations and interlevel transfers, we extract fundamental parameters such as the rate of spontaneous emission, the bright and dark state splitting, the activation energy of nonradiative channels, and the capture time. Many parameters describing the exciton dynamics are quantified for the first time.

The article is organized as follows. First, we describe the nature of the samples and the effect of the IC symmetry of the excitonic fine structure. Then, we present the temperature evolution of the recombination rate for all IC configurations studied and a three-level population balance model allowing an

*philippe.st-jean@polymtl.ca

insightful analysis of the experimental data. Finally, we discuss the dynamical processes governing the exciton dynamics.

II. SAMPLES AND EXPERIMENTAL SETUP

Nitrogen δ -doped layers, inserted between a 1 μm GaP buffer and a 200 nm GaP cap, were grown by a low-pressure metal-organic chemical vapor deposition on undoped GaP(001) substrates. The nitrogen density of several δ -doped layers was measured by secondary ion mass spectroscopy. Extensive details on the growth technique and characterization of the samples are presented in Refs. [9,15]. The δ -doped layer that we used had a sheet density of 10^{11} cm^{-2} . Assuming a random nitrogen distribution, we estimate a dyad surface density of about $1 \mu\text{m}^{-2}$. However, this calculated value only provides an order of magnitude estimate of the dyad density, as the surface dynamics of adsorbed atoms and the nitrogen dyad formation energy could play an important role in determining their formation probability. The resolution of our diffraction-limited confocal microscope system ($\sim 2 \mu\text{m}^{-2}$) did not allow resolving single emitters. However, intensity fluctuations on the scale of a few μm suggest that the photoluminescence measurement averaging occurs over a relatively low number of dyads. Therefore, in contrast to previous work on nitrogen ICs in GaP [16–18], measurements presented in this work were obtained on small ensembles of emitters. Minimizing the number of emitters reduces inhomogeneous broadening and can lead to a more accurate analysis of the exciton dynamics.

Time-resolved photoluminescence (PL) measurements of exciton bounds to various nitrogen isoelectronic centers were performed at temperatures ranging from 5 to 60 K. Excitation was provided by a frequency-doubled 1 ps mode-locked Ti:sapphire laser set at 840 nm. To access relatively long lifetimes, the laser repetition rate was reduced to 8 MHz using a pulse picker. The time dependence of the PL signal was analyzed using a spectrometer with a spectral resolution of 50 μeV and an avalanche photodiode with a time resolution of less than 50 ps. A motorized $\lambda/2$ wave plate and a polarizer were used to analyze the polarization of the emission.

III. IC CONFIGURATIONS AND EXCITONIC FINE STRUCTURES

The nitrogen ICs studied in this work are shown in Fig. 1. The A line corresponds to excitons bound to isolated nitrogen atoms and NN_i refers to exciton bound to nitrogen dyads of various interatomic separations and symmetries. This assignment follows the one proposed in Ref. [13], where the lowest energy transition (NN_1) is assigned to nearest-neighbor nitrogen atoms on the anionic sublattice. At higher energies, we observe the third nearest-neighbour dyad (NN_3), the fourth (NN_4), the sixth (NN_6), and, finally, the single-atom configuration at 2.316 eV. The fine structure of each configuration is described in the following section. We do not observe transitions associated with NN_2 and NN_5 in these δ -doped layers. We attribute this to their particular configuration [14] and symmetry [13,19], which remain to be unambiguously determined from single-emitter studies.

The excitonic fine structure is determined by the electron-hole exchange interaction, which splits bright $J = 1$ triplet

states and dark $J = 2$ quintuplet states, and the crystal field in the vicinity of the isoelectronic center which splits and mixes bright and dark states. The observed fine structure is uniquely determined by the symmetry of the center and can be accurately modeled using an invariant expansion [20]. The symmetry of dyad configurations was previously analyzed [19] and our polarization-resolved PL measurements are consistent with these identifications. Because of the crystal field, the exciton total angular momentum J does not provide a rigorous description of quantum states and symmetry-adapted representations should be used [20]. However, since the exchange interaction dominates the crystal field, we use the notation “ $J = 1$ ” or “ $J = 2$ ” to bring out the main component of these mixed states. This will be helpful for the discussion of the relative oscillator strength and the lifetime of various states.

The T_d symmetry of the single nitrogen atom configuration in GaP does not lift the degeneracy of the “ $J = 1$ ” triplet states and only a single bright and unpolarized transition (A line) is observed. “ $J = 2$ ” states split into a doublet and a triplet and both states are not radiatively coupled to the ground state. However, at very low temperatures, previous works have measured a single unresolved and unpolarized transition associated with these “ $J = 2$ ” states (B line). The presence of this transition is attributed to the spontaneous emission that becomes faster than the thermally activated exciton transfer to higher energy bright states. It remains unclear whether this emission arises from a quadrupole transition or a local symmetry perturbation.

Due to their lower symmetry, the fine structure of dyads is richer. For instance, NN_1 is of C_{2v} symmetry and the degeneracy of all excitonic states is lifted, leading to a fine structure composed of 8 individual states: one set of states ($B_{X,Y,Z}$) leading to *bright* transitions, one set ($W_{X,Y,Z}$) leading to relatively *weak* transitions, and two unobservable *dark* states ($D_{1,2}$). All allowed transitions are linearly polarized and the subscripts X , Y , and Z represent polarizations along $[110]$, $[1\bar{1}0]$, and $[001]$, respectively. However, in a δ -doped layer, dyads are preferentially formed in the (001) plane; therefore, dyads are predominantly oriented along $[110]$ or $[1\bar{1}0]$, implying that only four out of the six transitions can be observed: $B_{X,Y}$ and $W_{X,Y}$. Similarly, NN_4 , for which a C_{2v} symmetry has also been predicted, only shows four transitions.

Figures 2(a) and 2(b) show the intensity of these four transitions as a function of energy and linear polarization angle at 4 K. Two bright transitions are observed at high energy ($B_{X,Y}$) and two weak transitions ($W_{X,Y}$) at lower energies. The intensity difference can be explained by considering the dominant angular momentum component of these four states. The high-energy states $B_{X,Y}$ evolved directly from “ $J = 1$ ” states and therefore have a strong allowed component. In contrast, $W_{X,Y}$ evolved from “ $J = 2$ ” states and have become allowed by the mixing of some “ $J = 1$ ” component induced by the low-symmetry crystal field associated with the dyad. The last two states, $D_{1,2}$, do not mix and remain strictly forbidden. Their spectral position is unknown, but the analysis of the PL dynamics will reveal that they are below $W_{X,Y}$ and that their energy position depends on the interatomic separation of the dyad.

The relative intensity of B and W transitions depends on temperature. At 30 K, the PL spectra of NN_1 shown in Figs. 2(c) and 2(d) reveal that only $B_{x,y}$ transitions can be

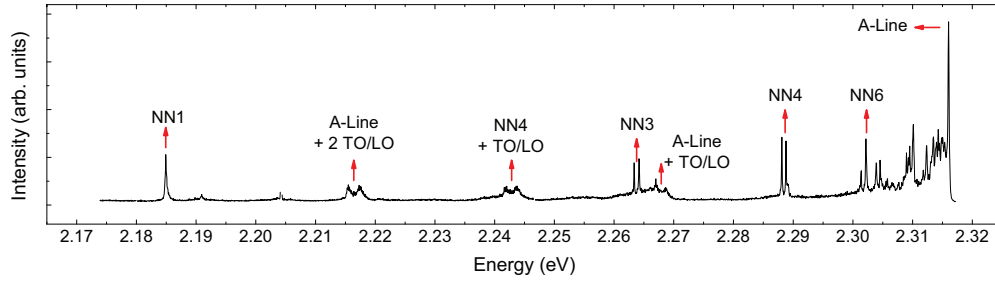


FIG. 1. (Color online) Photoluminescence spectrum measured at 30 K. The sharp lines correspond to the emission from ICs: single-atom configuration (A line) and dyads (NN_i). Phonon replica of the A line and NN_4 are also observed.

observed. The complete evolution of the intensity of $B_{X,Y}$ and $W_{X,Y}$ transitions with temperature is presented in Fig. 2(e). Similarly to the case of the isolated nitrogen low-energy B line, the rapid quenching of the low-energy transitions W with temperature can be explained by a fast and effective exciton transfer, activated by temperature, to high-energy bright states. Above 30 K, the intensity of $B_{X,Y}$ decreases because of thermally activated nonradiative processes that will be discussed in the next sections.

Similar results were obtained for all other dyad configurations: sets of bright and weak transitions separated by about 1 meV were observed at low temperatures while at higher temperatures only bright transitions remained.

As mentioned earlier, the nitrogen dyad surface density was slightly above the highest density that could be optically resolved. Accordingly, no polarization contrast was expected from measurements on small ensembles of randomly oriented nitrogen dyads along equivalent crystallographic directions. The large polarization contrast observed for all transitions associated with NN_1 (shown in Fig. 2) and NN_3 (not shown) likely results from the nonequivalence between the $[110]$ and $[1\bar{1}0]$ directions in the surface dynamic during nitrogen deposition and diffusion. Similar effects have been reported for MBE-grown III-V and II-VI semiconductors [21] and for nearest-neighbor Te dyads in δ -doped ZnSe layers [10].

Interestingly, as the internuclear separation between the nitrogen atoms increases, the linear polarization contrast decreases due to a randomization of dyad orientation [22]. This explains why the four transitions from NN_4 (not shown), for which a C_{2v} symmetry is predicted, do not show a significant degree of polarization comparatively to NN_1 . As already reported [22,23], the fine structure from NN_6 (C_{3v} symmetry) is composed of a single unpolarized transition, but it is impossible to attribute this absence of polarization to the higher symmetry of this configuration or to a randomization of the orientations.

IV. EXCITONIC RECOMBINATION REGIMES

We proceed with the description of the time dependence of the photoluminescence. The first important aspect is that all transitions composing the excitonic fine structure exhibited exactly the same time dependence. For example, the dynamics of all four transitions shown in Fig. 2(a) for NN_1 were independently measured and were found to be identical at every temperature. This was also the case for all other dyads studied. This result indicates that the transfer rate

between these states is much faster than the radiative lifetimes associated with each of these levels. This allows us to easily compare the recombination dynamics of various nitrogen dyads using only one decay curve for every configuration. Furthermore, in contrast with previous measurements made on samples with much higher nitrogen concentrations, the lifetime did not exhibit any variation with excitation intensity [16].

Figure 3(a) shows the measured decay time of the luminescence from NN_6 at 10, 28, and 60 K. To extract quantitative information, these intensity curves were modeled with the sum of an exponential rise term and a biexponential decay (red curves). Three characteristics times were thus obtained: the rise time τ_r , the short decay time τ_s , and the long decay time τ_l . The rise time, representing the characteristic time of capture of the exciton, ranges between 400 ps and 600 ps. This capture time is not affected by temperature and does not vary with the dyad configuration. However, the time dependence of the intensity varies significantly with temperature. At $T = 10$ K, a biexponential behavior is clearly observed with a short decay time (τ_s) of 3.0 ns and a longer decay time (τ_l) of 176 ns. As temperature is increased to 28 K, two effects are easily noticed. First, the short decay component is overtaken by the long decay component and a monoexponential decay is observed. Second, the long decay time quickly drops from 176 ns to 16.5 ns. At 60 K, τ_l is further reduced and reaches a maximal value of 0.4 ns, which is very similar to the rise time.

The temperature evolution of the recombination rate attributed to the longer decay ($\Gamma_l = \frac{1}{\tau_l}$) is presented in panel (b) of Fig. 3. As temperature is raised from 5 to 60 K, three distinct regimes are clearly observed. In regime I, at lowest temperatures, a biexponential decay is observed. Upon increasing the temperature, the importance of τ_s quickly vanishes and τ_l dominates. As shown in Fig. 3(b), the emission rate $\Gamma_l = \tau_l^{-1}$ increases relatively slowly up to 25 K. This behavior is typical of a recombination dynamic driven by thermally mixed allowed and forbidden states, as has been observed for isolated CdSe quantum dots [24] and Te ICs in ZnSe [10]. A theoretical model describing the origin of both the slow and the fast components has been developed by Labeau *et al.* [24]. However, in contrast with these two systems, our system involves degenerate heavy- and light-hole bands and twice the number of levels participate in the time dynamics. Furthermore, the temperature evolution of the intensity of the different transitions forming the fine structure [Fig. 2(e)] clearly shows that a transfer between B and W states cannot be neglected and that it has to be taken into account. Therefore, a more complete model is necessary to properly describe our

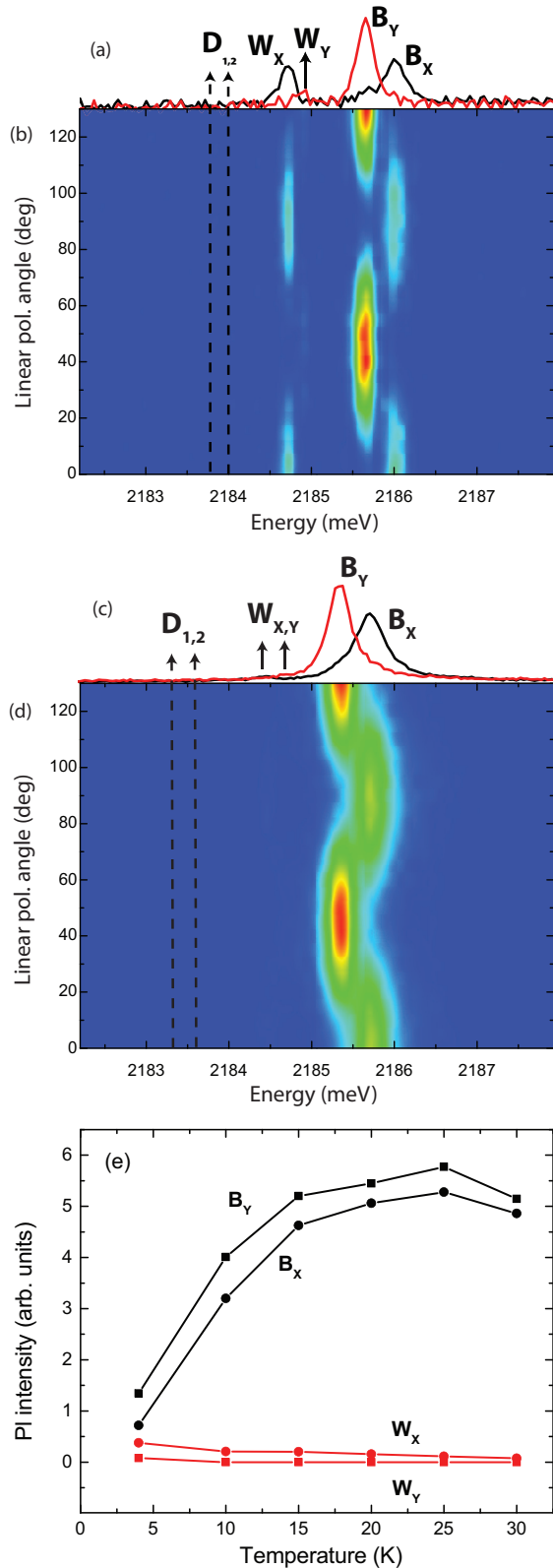


FIG. 2. (Color online) PL intensity as a function of energy and polarization for dyad NN_1 at (a), (b) $T = 4$ K and (c), (d) $T = 30$ K. The attribution of all excitonic transitions is presented in panels (a) and (c) where the black and red curve spectra show the PL polarized at 0° and 90° , respectively. (e) PL intensity as a function of temperature for bright ($B_{x,y}$) and weak ($W_{x,y}$) transitions. Dark transitions ($D_{1,2}$) are not observed.

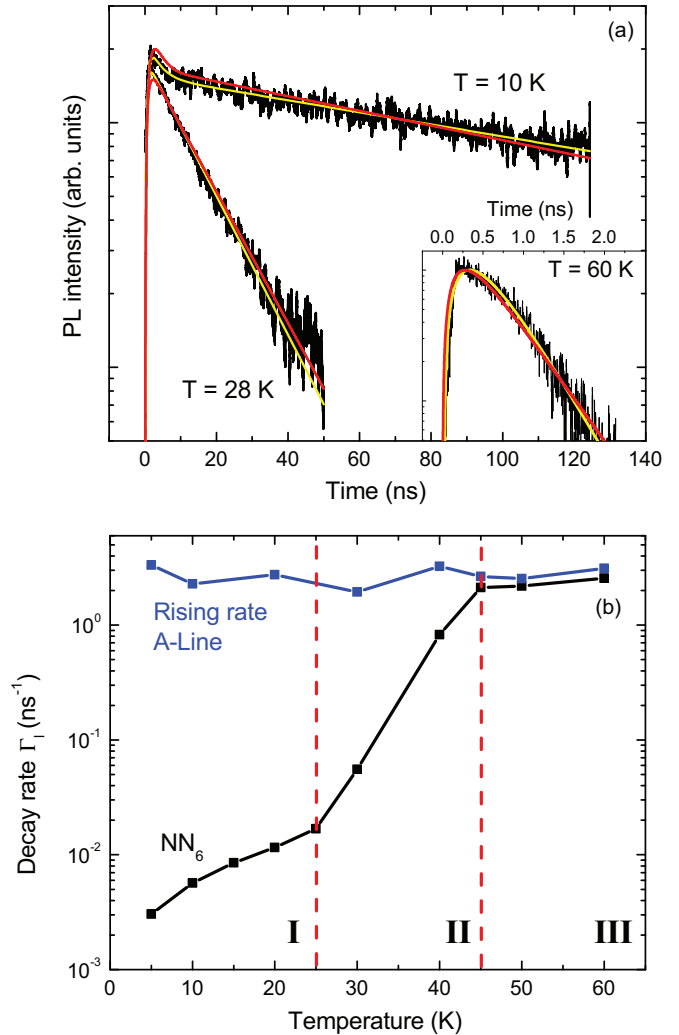


FIG. 3. (Color online) (a) Temporal dependence of the PL intensity of NN_6 at $T = 10, 28,$ and 60 K. The red curves represent a single exponential intensity rise followed by a single- or biexponential decay and the yellow curves represent calculated PL decay curves, obtained by the balance of populations model presented in Sec. V, that best fitted the data. (b) The black curve shows the emission rate, $\Gamma_l = \tau_l^{-1}$, of NN_6 as a function of temperature and the blue curve shows the inverse of the rise time of the PL from excitons bound to isolated nitrogen atoms (A line). The vertical lines separate the three PL decay regimes discussed in the text.

data, which will be presented in the next section. Minimizing the nitrogen concentration and the number of emitters appears crucial for an accurate analysis of time dynamics. For example, previous time-resolved PL experiments [16–18] could not observe biexponential decays, therefore making it impossible to adequately model the interlevel dynamics of excitons.

In regime II, the time decay of the luminescence is monoexponential and, as a function of temperature, Γ_l increases exponentially. This increase is associated with the thermal-activation of competing recombination mechanisms. To explain the quenching of the luminescence intensity with temperature [25], three mechanisms were suggested: (1) the escape of the whole exciton, (2) the escape of the loosely bound hole, leaving a single bound electron, and (3) the complete

unbinding of the exciton, resulting in a free electron and a free hole. The analysis of the data with the model presented in the next section will allow extracting an activation energy and determination of the dominant mechanism as a function of the dyad interatomic separation.

Finally, in the third regime, a plateau is observed as Γ_I reaches a maximum value of 2.5 ns^{-1} , corresponding to a lifetime of 400 ps. This lower lifetime limit coincides with the rise time of the luminescence of the A line. This suggests that, in regime III, the recombination dynamics of NN_6 is dominated by the capture of excitons by single-atom ICs followed by their hopping to the dyad. Hopping between nitrogen dyads has already been observed [26] and it has been demonstrated that hopping from single nitrogen atoms is an important populating mechanism of dyads [27–29]. Although hopping in GaP:N is efficient for a distance over at least 10 nm, the very low dyad density of our samples makes interdyad hopping negligible. However, as the nitrogen surface density is three orders of magnitude higher, hopping from single-atom ICs is most likely.

V. TIME DYNAMICS MODEL

A population balance model is developed to analyze and explain the time dynamics of the photoluminescence intensity as a function of the temperature. To reduce complexity and limit the number of parameters required, the proposed model groups into a single level all excitonic states with similar characteristics, therefore requiring three independent excitonic levels instead of eight. These levels and the population transfer processes considered are shown in Fig. 4.

The first level B is formed from the three bright states $B_{X,Y,Z}$ located at high energy, the second level W is formed from the three weak states $W_{X,Y,Z}$ of intermediate oscillator strength and located exactly E_{BW} below B (this value is extracted from the PL spectra), and the third level D is formed from the two dark states $D_{1,2}$. The energy position of these dark states E^{BD} is not known and will be determined from the experimental decay curves.

The following arguments are used to justify this simplification. The similar decay rates from all excitonic transitions indicate that fast interlevel transfers ($B \leftrightarrow D$, $B \leftrightarrow W$, $W \leftrightarrow$

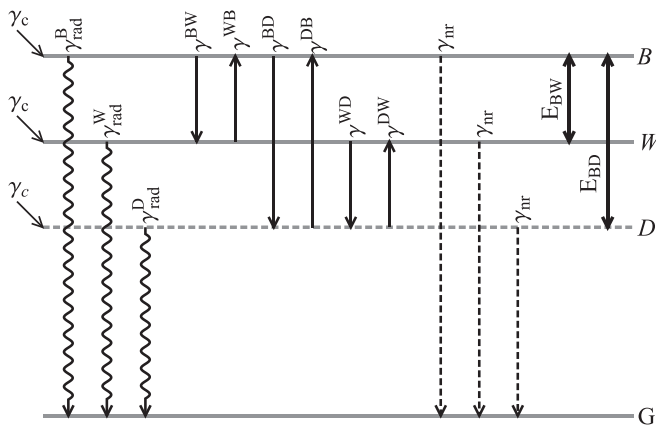


FIG. 4. Three-level model used for the analysis of the exciton dynamics. All transfer processes considered (γ) are described in the text and E refers to energy difference between the three excited levels.

D) occur before radiative emission. By mixing sets of levels well separated in energy, these fast transfers minimize thermal population difference between $B_{X,Y,Z}$ and $W_{X,Y,Z}$ sublevels that could be present at low temperatures. The PL intensity as a function of temperature presented in Fig. 2(e) supports this assumption. Assuming that the population of a state is proportional to the product of the PL intensity and lifetime [24], similar intensities and lifetimes indicate that both $B_{X,Y,Z}$ and $W_{X,Y,Z}$ sublevels are similarly populated. Since this behavior was observed from all other dyad configurations and at all temperatures, grouping sublevels together represents a reasonable assumption allowing an analysis that would otherwise require a large number of adjustable parameters.

Populations in these three levels (n_B , n_W , and n_D) evolve with time according to the following balance equations,

$$\begin{aligned} \frac{dn_B}{dt} &= -(\gamma_{\text{rad}}^B + \gamma_{\text{nr}} + \gamma^{BW} + \gamma^{BD})n_B \\ &\quad + \gamma^{WB}n_W + \gamma^{DB}n_D + \gamma_c n_0, \\ \frac{dn_W}{dt} &= -(\gamma_{\text{rad}}^W + \gamma_{\text{nr}} + \gamma^{WB} + \gamma^{WD})n_W \\ &\quad + \gamma^{BW}n_B + \gamma^{DW}n_D + \gamma_c n_0, \\ \frac{dn_D}{dt} &= -(\gamma_{\text{rad}}^D + \gamma_{\text{nr}} + \gamma^{DB} + \gamma^{DW})n_D \\ &\quad + \gamma^{BD}n_B + \gamma^{WD}n_W + \gamma_c n_0, \end{aligned} \quad (1)$$

where n_0 represents the population of photogenerated carrier and γ_c represents the rate at which an IC captures an exciton. γ_{rad}^B , γ_{rad}^W , and γ_{rad}^D are the rates of spontaneous emission of the three levels. The rate of thermally activated nonradiative processes γ_{nr} is given by

$$\gamma_{\text{nr}}(T) = \gamma_{\text{nr}}^0 \left(\frac{1}{\exp(E_{\text{nr}}/k_B T) - 1} \right), \quad (2)$$

where γ_{nr}^0 is a characteristic rate and E_{nr} is the activation energy, which we will both assume equal for all three levels. The transfer rate from low-energy level i to a high-energy level j through spin-flip processes is given by

$$\gamma^{ij}(T) = \gamma^0 \left(\frac{1}{\exp(E_{ij}/k_B T) - 1} \right) \quad (3)$$

and the transfer rate for a high-energy level j to a low-energy level i is $\gamma^{ji}(T) = \gamma^{ij}(T) + \gamma^0$. γ^0 is assumed constant for all levels and E_{ij} is the energy separation between levels i and j .

Numerical solutions to this system of differential equations allows calculating the PL decay curves as a function of temperature. The free parameters are γ_{capt} , mainly dependent on the rising edge of the PL, and $\gamma_{\text{rad}}^{B,W,D}$, γ_{nr}^0 , E_{nr} , γ^0 , and the energy splitting between B and D , E_{BD} , mostly dependent on the decay of the PL.

For a given IC configuration, the values for these parameters were determined by *simultaneously* fitting all PL decay curves obtained between 5 and 60 K. Figure 3(a) compares the experimental and the numerical PL decay curves for NN_6 (yellow curves) for temperatures located in each of the three regimes discussed earlier. As can be seen, a single set of parameters reproduces all the important characteristics of

TABLE I. Experimental values describing the exciton dynamics. The capture rate ranged between 400 and 600 ps and did not vary with temperature or IC configuration. For the single-atom configuration, the *weak* states (B line) was not observed.

ICs	Energy (eV)	γ_{rad}^B (10^7 s^{-1})	γ_{rad}^W (10^6 s^{-1})	γ_{rad}^D (10^4 s^{-1})	γ_{nr}^0 (10^{12} s^{-1})	E_{nr} (meV)	γ^0 (10^{10} s^{-1})	E_{BD} (meV)	E_{WD} (meV)
A line	2.3171	2.3		≤ 1	0.5	13.9	0.04	0.6	
NN ₆	2.3035	5.3	0.95	≤ 1	0.33	21.3	0.02	1.2	0.6
NN ₄	2.2891	5.0	1.0	≤ 1	2.8	38.2	2.7	1.4	0.7
NN ₃	2.2645	6.1	1.5	≤ 1	1.9	41.5	6.1	1.5	0.8
NN ₁	2.1850	5.8	1.0	≤ 1	2.5	44.2	1.0	2.1	1.0

the decay curves measured at 10, 28, and 60 K and for all other temperatures studied (not shown). The parameters extracted for NN₆ and all other IC configurations are presented in Table I. Although the number of extracted parameters may appear relatively large, their determination from a fit involving about 10 individual PL decay curves spanning a wide temperature range allowed extracting reliable values. Furthermore, the decay curve proved quite sensitive to each parameter and no other meaningful sets of values could be found, indicating that this approach is robust and accurate.

The long rate of emission, Γ_l , is extracted from calculated curves for each IC configurations studied and presented as the continuous lines in Fig. 5(b). As can be observed, the temperature variation of the decay rate of NN₆ first presented in Fig. 3(b) and that of NN₁, NN₃, and NN₄ are extremely well represented. This excellent agreement indicates that the model proposed and its underlying assumptions capture all important aspects of the carrier dynamics, which is discussed next, as a function of the IC configuration.

VI. DISCUSSION ON THE PROCESSES GOVERNING THE DYNAMICS

Table I reveals that similar values for spontaneous emission rates γ_{rad} were obtained for all IC configurations and that no

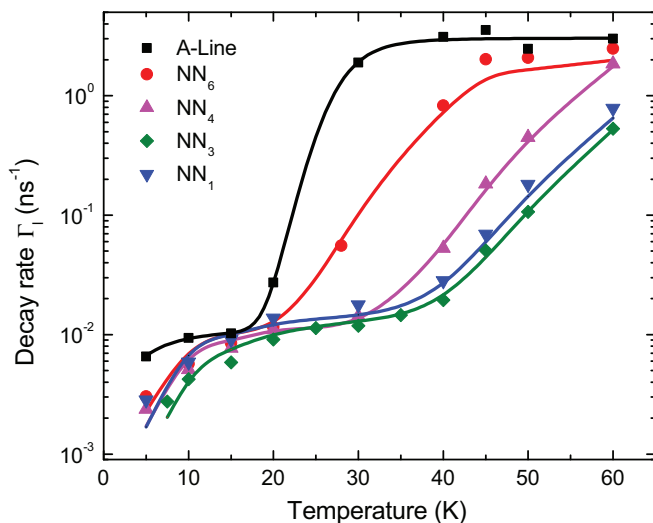


FIG. 5. (Color online) Temperature dependence of the emission rate, $\Gamma_l = \tau_l^{-1}$, traced on the experimental (symbols) and calculated (lines) PL decay curves for all IC configurations.

significant dependence on the interatomic separation can be identified. The spontaneous lifetime is about 18 ns for *B* states, 0.90 μs for *W* states, and superior to 100 μs for *D* states. In agreement with previous PL intensity measurements [13], *B* states have an oscillator strength about an order of magnitude stronger than *W* states. As expected, the oscillator strength of *D* states is so small relatively to *W* and *B* states that any values under $1 \times 10^4 \text{ s}^{-1}$ lead to satisfactory results.

Energy E_{nr} is directly related to the mechanism responsible for the intensity reduction with temperature and its value can be used to identify it. Table I shows that these activation energies are more than one order of magnitude greater than the energy splitting between levels forming the fine structure. This confirms our earlier hypothesis that, in first approximation, all the excitonic states of an IC are equally affected by the nonradiative process and that a single parameter (γ_{nr}^0) can be used for all excitonic levels.

For ICs with the lowest interatomic separations and highest binding energies (NN_{1,3,4}), activation energies between 38 and 44 meV are obtained. In contrast, the value for NN₆, 21 meV, is significantly lower and is about half that of configurations with larger interatomic separation. This difference in activation energy points to two distinct PL quenching mechanisms [25,30]. For dyads of low interatomic separations, the binding energy of the localized electron is relatively large and the activation energy measured is associated with the escape of the Coulomb-bound hole [25], with the electron remaining bound to the dyad. For dyads of large interatomic separations and single-atom centers, the activation energy E_{nr} is close to the optical binding energy, indicating that the whole exciton escapes.

Although the escape mechanism for NN_{1,3} has already been identified as hole escape, which is consistent with our findings, no clear identification of the mechanisms associated with shallower centers has been made yet. References [25] and [30] have respectively identified hole escape and exciton escape as the mechanisms governing NN₄, and both have tentatively suggested exciton escape for NN₆. Our results clearly indicate that the quenching of NN₄ is dominated by hole escape while that of NN₆ is dominated by exciton escape. From NN₁ to NN₄, the hole binding energy decreases by 6 meV, because, as the dyad interatomic separation increases, the electron localization decreases and so does the strength of the Coulomb interaction between the electron and the hole.

The bright and dark states splitting (E_{bd}) is 0.6 meV for single-nitrogen ICs. As mentioned earlier, this exchange splitting is expected to be larger for dyads and should increase as the internuclear distance decreases, as theoretically

predicted by Gil *et al.* [23]. The data of Table I reveals that this is indeed the case: the splitting increases from 1.2 meV for NN_6 to 2.1 meV for NN_1 . The exchange interaction is inversely proportional to the confinement volume [31], and since the hole binding energy and potential do not vary significantly for NN_{1-4} , the hole wave function is not affected and the magnitude of the splitting can thus be related to the extension of the electron wave function. With this analysis, the data clearly indicate that the electron wave functions are significantly more localized for dyads than for single-atom ICs. Finally, this localization increases significantly as the interatomic separation decreases.

As initially assumed from the similar lifetimes for all transitions composing the fine structure of a given IC configuration, interlevel transfer rates dominate spontaneous emission rates. For high (NN_6 and A line) and low ($NN_{1,3,4}$) interatomic separation configurations, γ^0 exceeds γ_{rad}^B by one and three orders of magnitude, respectively. This indicates that one or more spin-flip mechanisms efficiently randomize excitonic states. These may include hyperfine interaction between the electron and nuclei [32], electron-hole exchange interaction [33], deformation-potential interaction described by the Bir-Pikus Hamiltonian [34], spin-orbit coupling [35], and electrical interaction with neighboring charges [36]. However, it has been demonstrated that spin-flip mediated by phonon-assisted spin-orbit interaction is suppressed in strongly confined quantum dots [37]. Also, transfer rates between dark and bright states in quantum dots, due to the interplay of the exchange interaction and the Bir-Pikus Hamiltonian, were estimated to be very large ($T > 150$ ns) [34,38], compared to the exciton lifetime. Therefore, it is believed that hyperfine interaction or influence of neighboring charges likely dominate the interlevel transfer of excitons in this system.

In the discussion of the decay rate of NN_6 in regime III, we suggested that dyads are populated through the fast hopping of excitons from single-nitrogen ICs since the decay rate of NN_6 plateaus at a value corresponding to the rise time of the A line [see Fig. 3(b)]. The calculated decay rates, presented in Fig. 5, clearly show this behavior for NN_6 . For dyads with a larger binding energy, the activation energy of hopping from single-nitrogen ICs is superior and higher temperatures would be necessary to unambiguously conclude that it is the dominating capture mechanism of excitons.

VII. CONCLUSION

In conclusion, we presented an extensive study of the recombination dynamics of excitons bound to nitrogen isoelectronic centers in GaP formed by single-atom and two-atom isoelectronic centers. For all ICs studied, the temperature dependence of the decay times clearly exhibits three different regimes where the dynamics is dominated by (1) thermally activated transfer between the different excitonic states forming the fine structure at low temperatures, (2) thermally activated nonradiative channel of emission at intermediate temperatures, and (3) a fast hopping from the single-atom configuration to dyads at high temperatures. By fitting the data with PL decay curves calculated with a balance of populations model we were able to extract the fundamental parameters governing these three regimes: the time of capture of excitons, the rate of spontaneous emission of all excitonic states forming the fine structure, the dark and bright state splitting, and the activation energies of nonradiative processes. Most of these parameters were calculated for the first time and the precise values of the activation energies of the nonradiative processes allowed a clarification of their nature which is the escape of the hole for $NN_{1,3,4}$ and the transfer to a free excitonic state for NN_6 and the A line.

These findings suggest that nitrogen ICs are interesting candidates for classical single-electron memories of atomic dimensions. Since the hole binding energy is significantly less than that of the electron for $NN_{1,3,4}$, a relatively weak electric field could be applied to break the exciton and expel the hole, leaving the electron in a long-lived metastable state until a hole is brought back to induce excitonic emission. On the other hand, the fast spin-flip mechanisms observed represent an obstacle for the realization of exciton qubits. However, as the nature of these mechanisms is not yet understood, it remains to be determined whether their effect could be mitigated, as it has been demonstrated for example for the hyperfine interaction in quantum dots [39]. Interestingly, interlevel transfers do not play a similar role for nitrogen ICs in GaAs, indicating that different impurity-host combinations present remarkably different sets of characteristics. Other IC systems of interest that would likely provide advantageous coherence times include hole traps such as Te dyads in ZnSe and electron traps such as Be dyads in isotopically purified Si.

-
- [1] A. Boyer de la Giroday, N. Sköld, R. M. Stevenson, I. Farrer, D. A. Ritchie, and A. J. Shields, *Phys. Rev. Lett.* **106**, 216802 (2011).
 - [2] F. H. L. Koppens, C. Buizert, K. J. Tielrooij, I. T. Vink, K. C. Nowack, T. Meunier, L. P. Kouwenhoven, and L. M. K. Vandersypen, *Nature (London)* **442**, 766 (2006).
 - [3] G. D. Fuchs, G. Burkard, P. V. Klimov, and D. D. Awschalom, *Nat. Phys.* **7**, 789 (2011).
 - [4] P. C. Maurer, G. Kucsko, C. Latta, L. Jiang, N. Y. Yao, S. D. Bennett, F. Pastawski, D. Hunger, N. Chisholm, M. Markham, *et al.*, *Science* **336**, 1283 (2012).
 - [5] M. Steger, K. Saedi, M. L. W. Thewalt, J. J. L. Morton, H. Riemann, N. V. Abrosimov, and P. Becker, *Science* **336**, 1280 (2012).
 - [6] J. J. Pla, K. Y. Tan, J. P. Dehollain, W. H. Lim, J. J. L. Morton, D. N. Jamieson, A. S. Dzurak, and A. Morello, *Nature (London)* **489**, 541 (2012).
 - [7] S. Francoeur, J. F. Klem, and A. Mascarenhas, *Phys. Rev. Lett.* **93**, 067403 (2004).
 - [8] M. Jo, T. Mano, T. Kuroda, Y. Sakuma, and K. Sakoda, *Appl. Phys. Lett.* **102**, 062107 (2013).
 - [9] Y. Sakuma, M. Ikezawa, M. Watanabe, and Y. Masumoto, *J. Cryst. Growth* **310**, 4790 (2008).

- [10] A. Muller, P. Bianucci, C. Piermarocchi, M. Fornari, I. C. Robin, R. André, and C. K. Shih, *Phys. Rev. B* **73**, 081306 (2006).
- [11] S. Marcet, R. André, and S. Francoeur, *Phys. Rev. B* **82**, 235309 (2010).
- [12] S. Marcet, C. Ouellet-Plamondon, G. Éthier-Majcher, P. Saint-Jean, R. André, J. F. Klem, and S. Francoeur, *Phys. Rev. B* **82**, 235311 (2010).
- [13] D. G. Thomas and J. J. Hopfield, *Phys. Rev.* **150**, 680 (1966).
- [14] B. Gil and H. Mariette, *Phys. Rev. B* **35**, 7999 (1987).
- [15] M. Ikezawa, Y. Sakuma, and Y. Masumoto, *Jpn. J. Appl. Phys.* **46**, L871 (2007).
- [16] H. D. Wolf, K. Richter, and C. Weyrich, *Solid State Commun.* **15**, 725 (1974).
- [17] I. K. Kristensen, *Phys. Scr.* **25**, 860 (1982).
- [18] J. Zheng and W. M. Yen, *J. Lumin.* **39**, 233 (1988).
- [19] B. Gil, J. Camassel, J. P. Albert, and H. Mathieu, *Phys. Rev. B* **33**, 2690 (1986).
- [20] S. Francoeur and S. Marcet, *J. Appl. Phys.* **108**, 043710 (2010).
- [21] M. D. Pashley, K. W. Haberern, W. Friday, J. M. Woodall, and P. D. Kirchner, *Phys. Rev. Lett.* **60**, 2176 (1988).
- [22] M. Ikezawa, Y. Sakuma, M. Watanabe, and Y. Masumoto, *Phys. Status Solidi C* **6**, 362 (2009).
- [23] B. Gil, J. Camassel, P. Merle, and H. Mathieu, *Phys. Rev. B* **25**, 3987 (1982).
- [24] O. Labeau, P. Tamarat, and B. Lounis, *Phys. Rev. Lett.* **90**, 257404 (2003).
- [25] M. D. Sturge, E. Cohen, and K. F. Rodgers, *Phys. Rev. B* **15**, 3169 (1977).
- [26] P. J. Wiesner, R. A. Street, and H. D. Wolf, *Phys. Rev. Lett.* **35**, 1366 (1975).
- [27] P. Leroux-Hugon and H. Mariette, *Phys. Rev. B* **30**, 1622 (1984).
- [28] Q. Hong, K. Dou, and X. Zhang, *Phys. Rev. B* **41**, 1386 (1990).
- [29] M. Felici, A. Polimeni, A. Miriametro, M. Capizzi, H. P. Xin, and C. W. Tu, *Phys. Rev. B* **71**, 045209 (2005).
- [30] E. Cohen and M. D. Sturge, *Phys. Rev. B* **15**, 1039 (1977).
- [31] T. Takagahara, *Phys. Rev. B* **62**, 16840 (2000).
- [32] H. Kurtze, D. R. Yakovlev, D. Reuter, A. D. Wieck, and M. Bayer, *Phys. Rev. B* **85**, 195303 (2012).
- [33] E. Tsitsishvili, R. Baltz, and H. Kalt, *Phys. Rev. B* **67**, 205330 (2003).
- [34] E. Tsitsishvili and H. Kalt, *Phys. Rev. B* **82**, 195315 (2010).
- [35] V. N. Golovach, A. Khaetskii, and D. Loss, *Phys. Rev. Lett.* **93**, 016601 (2004).
- [36] J. M. Smith, P. A. Dalgarno, R. J. Warburton, A. O. Govorov, K. Karrai, B. D. Gerardot, and P. M. Petroff, *Phys. Rev. Lett.* **94**, 197402 (2005).
- [37] A. V. Khaetskii and Y. V. Nazarov, *Phys. Rev. B* **64**, 125316 (2001).
- [38] K. Roszak, V. M. Axt, T. Kuhn, and P. Machnikowski, *Phys. Rev. B* **76**, 195324 (2007).
- [39] D. Stepanenko, G. Burkard, G. Giedke, and A. Imamoglu, *Phys. Rev. Lett.* **96**, 136401 (2006).